

Dissipation and amplification management in an electrical model of microtubules: Hybrid behavior network

Sedric Ndoungalah, Guy Roger Deffo, Arnaud Djine, and Serge Bruno Yamgoué
Citation: Chin. Phys. B, 2023, 32 (**11**): 110505. DOI: 10.1088/1674-1056/acc44f
Journal homepage: http://cpb.iphy.ac.cn; http://iopscience.iop.org/cpb

What follows is a list of articles you may be interested in

Analytical three-periodic solutions of Korteweg-de Vries-type equations

Mi Chen(陈觅) and Zhen Wang(王振)
Chin. Phys. B, 2023, 32 (**9**): 090504. DOI: 10.1088/1674-1056/acd9c4

Influence of the initial parameters on soliton interaction in nonlinear optical systems

Xinyi Zhang(张昕仪) and Ye Wu(吴晔)
Chin. Phys. B, 2023, 32 (**7**): 070505. DOI: 10.1088/1674-1056/ace1da

Breather and its interaction with rogue wave of the coupled modified nonlinear Schrödinger equation

Ming Wang(王明), Tao Xu(徐涛), Guoliang He(何国亮), and Yu Tian(田雨)
Chin. Phys. B, 2023, 32 (**5**): 050503. DOI: 10.1088/1674-1056/ac833d

Employment of Jacobian elliptic functions for solving problems in nonlinear dynamics of microtubules

Slobodan Zeković, Annamalai Muniyappan, Slobodan Zdravković, Louis Kavitha
Chin. Phys. B, 2014, 23 (**2**): 020504. DOI: 10.1088/1674-1056/23/2/020504

Folded localized excitations in the (2+1)-dimensional modified dispersive water-wave system

Lei Yan (雷燕), Ma Song-Hua (马松华), Fang Jian-Ping (方建平)
Chin. Phys. B, 2013, 22 (**1**): 010506. DOI: 10.1088/1674-1056/22/1/010506

Dissipation and amplification management in an electrical model of microtubules: Hybrid behavior network

Sedric Ndoungalah[1], Guy Roger Deffo[2,†], Arnaud Djine[1], and Serge Bruno Yamgoué[3]

[1] *Department of Physics, Faculty of Science, University of Bamenda, P.O. Box 39 Bamenda, Cameroon*

[2] *Research Unit of Automation and Applied Computers (UR-AIA), Department of Electrical Engineering, IUT-FV of Bandjoun, University of Dschang, BP 134, Bandjoun, Cameroon*

[3] *Department of Physics, Higher Teacher Training College Bambili, The University of Bamenda, P.O. Box 39 Bamenda, Cameroon*

(Received 6 January 2023; revised manuscript received 22 February 2023; accepted manuscript online 15 March 2023)

The control of dissipation and amplification of solitary waves in an electrical model of a microtubule is demonstrated. This model consists of a shunt nonlinear resistance–capacitance ($J(V)$–$C(V)$) circuit and a series resistance–inductance (R–L) circuit. Through linear dispersion analysis, two features of the network are found, that is, low bandpass and bandpass filter characteristics. The effects of the conductance's parameter λ on the linear dispersion curve are also analyzed. It appears that an increase of λ induces a decrease (an increase) of the width of the bandpass filter for positive (negative) values of λ. By applying the reductive perturbation method, we derive the equation governing the dynamics of the modulated waves in the system. This equation is the well-known nonlinear Schrödinger equation extended by a linear term proportional to a hybrid parameter σ, i.e., a dissipation or amplification coefficient. Based on this parameter, we successfully demonstrate the hybrid behavior (dissipation and amplification) of the system. The exact and approximate solitary wave solutions of the obtained equation are derived, and the effects of the coefficient σ on the characteristic parameters of these waves are investigated. Using the analytical solutions found, we show numerically that the waves that are propagated throughout the system can be dissipated, amplified, or remain stable depending on the network parameters. These results are not only in agreement with the analytical predictions, but also with the existing experimental results in the literature.

Keywords: microtubule, dissipation and amplification, hybrid behavior, solitary wave solutions

PACS: 05.45.Yv, 05.45.–a, 63.20.Pw **DOI:** 10.1088/1674-1056/acc44f

1. Introduction

Due to its great importance in various biological processes, protein dynamics has been widely studied in recent years.[1,2] Microtubules (MTs) are a typical example of such structures. They represent the main components of the cytoskeleton and play a crucial role in electrical activities within eukaryotic cells, including, for example, cellular division, intracellular information processing, regulation of synaptic inputs, modulation of neural firing, regulation of developmental plasticity, and mediation during transport of electrical signals.[3]

MTs are hollow cylinders formed by protofilaments aligned in directions parallel to their axis. The approximate values of their outer and inner radii are 25 nm and 15 nm, respectively.[4–6] Their lengths are of the order of micrometers or millimeters. Many theoretical and experimental studies have been envisaged to analyze their properties and dynamics. For instance, Priel *et al.* studied experimentally the electrodynamic properties of MTs.[7] The obtained results demonstrated that MTs are excellent conductors of electrical signals. They can also amplify an electric current stimulated by an applied voltage pulse. Through electroorientation experiments, Minoura and Muto found that the conductivity of the MT was 1500 mS/m, which was 15 times higher than that of the surrounding buffer.[8] Freedman *et al*. investigated ionic currents through microtubule nanopores.[9] The obtained results showed that the nanopores have asymmetric inner and outer conductances. Havelka *et al*. investigated multi-mode electro-mechanical vibrations of an MT.[10] They showed that electrically polar collective vibration modes of MTs lead to a quasi-periodic electric oscillating potential. Based on the kink solitons and breathers, Zdravkovic *et al*. explained the nonlinear dynamics of MTs.[11,12]

To better understand the dynamics of MTs and to elucidate their role in the electrical activities of cells, several electrical models of these biological systems have been proposed in the literature. In fact, since the pioneering work by Tuszynski *et al*. on nonlinear electrical transmission lines (NLTLs) modeling ionic wave propagation along actin filaments,[13] growing interest has been devoted to the use of NLTLs to mimic the behavior of MTs. For instance, the ionic-conduction properties of an MT have been investigated through a model of NLTL.[14] Ilic *et al*. used the same model to show that the localized ionic wave could be used to explain the behavior of MTs as biomolecular transistors capable of amplifying electrical information in neurons.[15] This model was

†Corresponding author. E-mail: guyrdeffo@yahoo.fr

© 2023 Chinese Physical Society and IOP Publishing Ltd

also exploited to describe the electrostatic potential coupled to the propagating localized waves along MTs.[16] Similar studies have also been conducted by Freedman *et al*. and Sataric *et al*. considering a two-dimensional electrical model[9] and an NLTL with negative resistive components,[17] respectively. Based on another model, these authors and other coworkers investigated the polyelectrolyte character of MTs.[18] A new NLTL model has also been introduced to investigate the creation and propagation of localized pulses of positive ions flowing along cellular MTs.[19] Recently, Ndjomatchoua *et al*. demonstrated that the electrical wave propagation in an MT could be modeled by a discrete NLTL including a cubic negative nonlinear resistance.[20] More recently, using an electrical model with strongly nonlinear resistive elements, Ghomsi *et al*. studied the capability of the inner part of an MT.[21] Other models of NLTLs mimicking the dynamics of MTs have also been realized.[22,23]

Analyzing the above cited works, we note that existing models to mimic the electrical behavior of MTs in the band-pass domain have only focused on the dissipative character of these systems. However, experimental evidence suggests that MTs act as biological electrical wires that can amplify electrical signals via the flow of condensed ion clouds. For instance, Priel *et al*. have shown that taxol-stabilized MTs behave as biomolecular transistors capable of amplifying electrical information.[7] In addition, this author and other coworkers obtained similar results by studying the effect of calcium on electrical energy transfer by MTs.[24] Hence, these works suggest that a complete description of the dynamics of the electrical bio-signals' propagation along MTs via a model of an NLTL can be made by taking into account both dissipation and amplification characteristics of MTs. To the best of our knowledge, such a study has not yet been considered.

In this paper, we aim to broaden the understanding of models of MTs as nonlinear electrical transmission lines with nonlinear resistive elements. Specifically, we undertake simultaneously herein the investigation of the amplification and the dissipation of electrical signals in an electrical model of MTs which is presented along with its exact dynamical equation in the next section. In Section 3, we first show that the dynamics of modulated waves in the network is governed by the standard nonlinear Schrödinger equation extended by a dissipation/amplification term. Next, the signs of various coefficients of this equation are studied. Finally, the baseband modulational instability of the amplitude equation is investigated. In Section 4, we investigate the exact and approximate solitary wave solutions of the governing equation. Analytical investigations of these obtained solutions are performed in Section 5. We conclude our paper in Section 6.

2. Model description and dynamic equation

2.1. Model presentation

The physical electrical model of a microtubule considered in the current paper is depicted in Fig. 1. It was described in some detail in Ref. [20] and consists of several identical blocks connected in sequence one to the other. Each block includes a shunt nonlinear conductance–capacitance $(J(V_n)$–$C(V_n))$ circuit and a series resistance–inductance (R–L) circuit. The first nonlinear element is a varicap diode whose differential capacitance $C(V_\mathrm{b}+V_n)=\mathrm{d}Q_n/\mathrm{d}V_n$ is a nonlinear function of the voltage V_n. For low voltages around the dc bias voltage V_b, $Q_n(V_n)$ at the (n)th node can be defined by[25,26]

$$Q_n = C_0\left(V_n - \alpha V_n^2 + \beta V_n^3\right), \tag{1}$$

where C_0 is the characteristic capacitance. α and β are positive real parameters. The second nonlinear element is negative nonlinear resistance satisfying the following expansion:[27]

$$J(V_n) = BV_n\left(V_n - d_1\right)\left(V_n - d_2\right). \tag{2}$$

In this relation, B is an amplitude factor determined by the slope at $V=0$ V. d_1 and d_2 are voltages which determine the zeros of J. For the active behavior of J, d_1 and d_2 have the opposite signs, while they are positive for the passive behavior of J.[27,28]

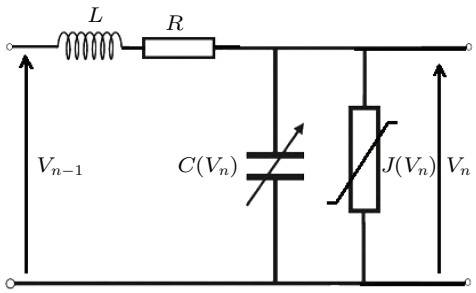


Fig. 1. Schematic representation of the electrical analogy of the MT model.

Considering $B_2 = B(d_1+d_2)$ and $B_1 = -Bd_1d_2$, relation (2) can be rewritten as

$$J(V_n) = BV_n^3 - B_2V_n^2 - B_1V_n.$$

Here, B_2 and B_1 represent the quadratic nonlinear and linear coefficients, respectively. The physical dimensions of B_1, B_2 and B are $[\Omega^{-1}]$, $[\Omega^{-1}\cdot \mathrm{V}^{-1}]$ and $[\Omega^{-1}\cdot \mathrm{V}^{-2}]$, respectively. Note that for $d_1=-d_2$, we obtain the expression of the negative nonlinear resistance effects of ionic flow through nanopores used in Refs. [20,21].

Applying Kirchhoff laws to the circuit of Fig. 1, the following differential equations governing the dynamics of signal voltage $(V_n(t))$ in the network are obtained:

$$\frac{\mathrm{d}^2}{\mathrm{d}t^2}\left(V_n - \alpha V_n^2 + \beta V_n^3\right) + u_0^2\left(2V_n - V_{n+1} - V_{n-1}\right)$$
$$+u_0^2\frac{\mathrm{d}}{\mathrm{d}t}\left(\gamma_1 V_n + \gamma_2 V_n^2 + \gamma_3 V_n^3\right)$$

$$+u_0^2\left(\beta_1 V_n^3-\alpha_1 V_n^2-4\lambda V_n\right)=0, \tag{3}$$

with $u_0^2=1/(LC_0)$, $\beta_1=RB$, $\alpha_1=RB_2$, $\lambda=RB_1/4$, $\gamma_1=(RC_0-LB_1)$, $\gamma_2=-(RC_0\alpha+LB_2)$, $\gamma_3=(LB+RC_0\beta)$ and $n=1,2,\ldots,N$. N represents the total number of blocks. In this study, numerical investigations are made for the following values of the network parameters:[16,27]

$$L=0.8\ \text{fH},\quad C_0=1.32\ \text{fF},\quad d_2=0.5\ \text{V},\quad d_1=-0.5\ \text{V},$$
$$\alpha=0.13\ \text{V}^{-1},\quad \beta=0.0197\ \text{V}^{-2},\quad B=0.125\ \text{mA/V}^3. \tag{4}$$

2.2. Linear dispersion law

The linear dispersion law of the model of Fig. 1 is derived and examined in this subsection. To this end, we consider the solution of Eq. (3) as $V_n=V_0\exp(\mathrm{i}(kn-\omega t))$ with V_0, k and ω representing the small wave amplitude, the wave number, and the angular frequency, respectively. Putting this solution into Eq. (3), and neglecting the terms of power greater than V_0 we obtain the angular frequency and group velocity associated with the wave packet as

$$\omega^2=4u_0^2\left[\sin^2\left(\frac{k}{2}\right)-\lambda\right],\quad \mu=\frac{\mathrm{d}\omega}{\mathrm{d}k}=\frac{u_0^2\sin(k)}{\omega}. \tag{5}$$

Equation (5) shows that our system is a band-pass filter. Nevertheless, we note that its allowed frequency band considerably depends on the sign of parameter λ which represents the nonlinear conductance's contribution to the angular frequency. Indeed, two cases can be distinguished.

For $\lambda>0$ ($d_1d_2<0$), Eq. (5) is valid if and only if the wave number k verifies the relation $k>k_c=2\arcsin\sqrt{\lambda}$. In this condition, the system is a low band-pass filter with lower cutoff frequency and upper cutoff frequency defined by $f_0=\omega(k_c)/(2\pi)=0$ and $f_c=\omega(\pi)/(2\pi)=2u_0\sqrt{1-\lambda}$, respectively. We note that the parameter λ can be used to decrease the bandwidth of allowed frequencies. Indeed, as we can see in Fig. 2(a) the dispersion curve changes considerably for different values of λ. We can also remark that the gap zone increases with λ. This result is more clearly seen in Fig. 3(a) where the bandwidth (f_c-f_0) of allowed frequencies as a function of the parameter is plotted as a function of λ.

For $\lambda<0$ ($d_1d_2>0$), Eq. (5) describes the band-pass filter character of the network. The corresponding upper cut-off and lower cut-off frequencies are defined by $f_0=\omega(0)/(2\pi)=2u_0\sqrt{-\lambda}$ and $f_c=\omega(\pi)/(2\pi)=2u_0\sqrt{1-\lambda}$, respectively. As we can clearly see in Fig. 2(b), the bandwidth of allowed frequencies also depends on the parameter λ. Figure 3(b) shows that cutoff frequencies f_0 and f_c decrease simultaneously with the growth of λ. In particular, a growth of λ increases the upper gap zone and decreases the lower gap zone. These results mean that the nonlinear conductance's contribution to the angular frequency can be used not only to change the bandwidth of allowed frequencies but also to facilitate the analysis of wave propagation in one forbidden band compared to the other.

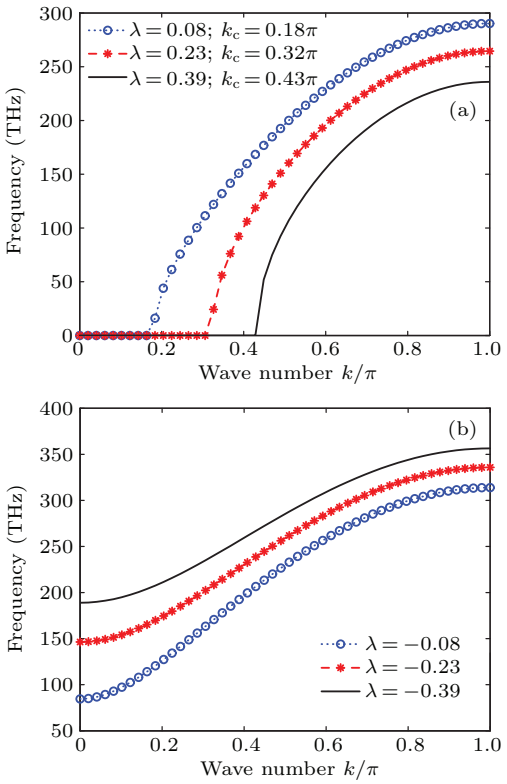


Fig. 2. Effect of the parameter λ on the linear dispersion curve of the network showing evolution of the frequency $f=\omega/(2\pi)$ as a function of the wave number k (rad/cell) with network parameters (4): (a) $d_2=-d_1$ ($\lambda>0$); (b) $d_2=d_1$ ($\lambda<0$).

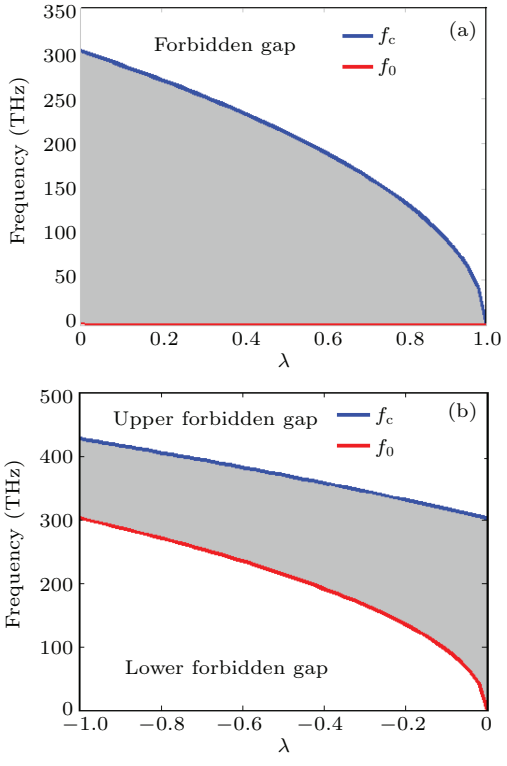


Fig. 3. Variation of the bandwidth of allowed frequencies as a function of the parameter λ with the network parameters (4): (a) $d_2=-d_1$ ($\lambda>0$); (b) $d_2=d_1$ ($\lambda<0$).

3. Extended nonlinear Schrödinger equation and baseband modulational instability

3.1. Extended nonlinear Schrödinger equation

This section is devoted to the derivation of the nonlinear equation describing the motion of nonlinear modulated waves in the MT electrical model of Fig. 1. Thus, we consider the reductive perturbation approach in the semidiscrete approximation. In this method, the carrier is treated with its discrete character and the envelope is described in the continuum approximation. Let us consider the voltage signal solution of Eq. (3) to be of the form[28]

$$V_n(t) = \varepsilon A(x,\tau)\,\mathrm{e}^{\mathrm{i}\theta} + \varepsilon^2 A_{20}(x,\tau) + \varepsilon^2 A_{22}(x,\tau)\,\mathrm{e}^{\mathrm{i}2\theta} + \mathrm{cc}, \quad (6)$$

where $\theta = kn - \omega t$ is the phase and cc stands for the complex conjugate of the preceding expression. ε is a small parameter. Solution (6) includes the fast local oscillation through the dependence of the phase θ, and then preserves the discrete character of the network, while the dependence of the envelope part described by $A(x,\tau)$ on the slow variables $\tau = \varepsilon^2 t$ and $x = \varepsilon(n - \mu t)$ takes care of the slow variation in amplitude. We then order the damping coefficient in Eq. (3) so that the damping and nonlinearity effects appear in the same perturbation equations. In particular, we assume that the dissipation effect of the network is weak. Thus, we consider that γ_1 is a perturbed parameter of order ε^2. Inserting Eq. (6) into Eq. (3), we obtain different equations as power series of ε.

First, the terms proportional to $\varepsilon\exp(\mathrm{i}\theta)$ and $\varepsilon^2\exp(\mathrm{i}\theta)$ give us, respectively, the angular frequency and group velocity obtained and investigated in the previous section.

Next, from the terms of order $[\varepsilon^2\exp(0\mathrm{i}\theta)]$ and $[\varepsilon^2\exp(2\mathrm{i}\theta)]$, we obtain, respectively, the continuous components $A_{20}(x,\tau)$ and the second harmonic $A_{22}(x,\tau)$ defined by

$$\begin{aligned} A_{20}(x,\tau) &= -\frac{\alpha_1}{2\lambda}\,|\,A(x,\tau)\,|^2, \\ A_{22}(x,\tau) &= \frac{-4\alpha\omega^2 + u_0^2\alpha_1}{4u_0^2(\sin^2(k) - \lambda) - 4\omega^2} A(x,\tau)^2. \end{aligned} \quad (7)$$

Finally, keeping terms of order ε^3, proportional to $\exp(\mathrm{i}\theta)$, we obtain the following nonlinear partial differential for $A(x,\tau)$:

$$\mathrm{i}\frac{\partial A}{\partial \tau} + P\frac{\partial^2 A}{\partial x^2} + Q\,|\,A\,|^2 A + \mathrm{i}\sigma A = 0. \quad (8)$$

This equation is a standard nonlinear Schrödinger equation (NLS) extended by a linear term. Its various coefficients are displayed below:

$$\begin{aligned} Q &= \frac{3(\beta\omega^2 - \beta_1 u_0^2)}{2\omega} + \frac{(u_0^2\alpha_1 - \omega^2\alpha)(Q_0 + Q_1)}{\omega}, \\ P &= \frac{\mu^2 - u_0^2\cos(k)}{-2\omega}, \\ Q_1 &= \frac{-4\alpha\omega^2 + u_0^2\alpha_1}{4u_0^2(\sin^2(k) - \lambda) - 4\omega^2}, \\ Q_0 &= -\frac{\alpha_1}{2\lambda}, \quad \sigma = \frac{u_0^2\gamma_1}{2}. \end{aligned} \quad (9)$$

Equation (8) includes the dissipation/amplification effect beside the linear group velocity dispersion (GVD) and the self phase modulation (SPM) represented, respectively, by the parameters P and Q. For instance, σ is the dissipation/amplification coefficient. It is due to the nonlinear and linear resistances respectively, in shunt and series branches of the network. From its expression, it is clearly observed that this coefficient is an explicit function of the nonlinear resistance parameters (B, d_1 and d_2) and can take any value and any sign depending on the considered values of these parameters and also of the magnitude of the resistance R. Hence, it becomes important to study its sign.

Specifically, since $u_0^2 > 0$, the nature (amplification or dissipation coefficient) of σ only depends on the sign of coefficient γ_1, which is an explicit function of the network's parameters. By definition, the coefficients L, C_0, R, and B are positive. Therefore, the sign and the nature of coefficient σ only depend on the sign of the parameters d_1 and d_2. Various combinations of these parameters have been used in the literature.[27]

For $d_1 d_2 < 0$, let

$$R_{\mathrm{cr}} = \frac{B_1 L}{C_0} = -\frac{BLd_1 d_2}{C_0}. \quad (10)$$

1. For $d_1 d_2 > 0$, we have $\sigma > 0$: in this case, σ is a dissipation coefficient.

2. For $d_1 d_2 < 0$ and $R > R_{\mathrm{cr}}$, we have $\sigma > 0$: in this case, σ is also a dissipation coefficient.

3. For $d_1 d_2 < 0$ and $R < R_{\mathrm{cr}}$, we have $\sigma < 0$: in this case, σ is an amplification coefficient.

4. For $d_1 d_2 < 0$ and $R = R_{\mathrm{cr}}$, we have $\sigma = 0$: in this case, the amplitude equation (8) leads to the well-known nonlinear Schrödinger equation. This result is in perfect agreement with existing results on the dissipative NLTL in which the dissipative terms of the NLS equation disappear when the dissipation elements (resistances) are not considered.[30–32] However, in contrast to these previous results, the dissipation is not neglected in the model studied in this paper. In other words, the resistance (R) always exists in our system but its effect is counterbalanced by the effect of the nonlinear conductance J. This new result shows clearly that the nonlinear resistance can be exploited to control the dissipation in the network of Fig. 1.

Although Eq. (8) has been derived in the context of NLTL mimicking the behavior of MTs, the well-known versatility of NLS type equations makes it legitimate to expect that its applications can extend beyond the NLTL. For instance, Okaly *et al.* derived a similar equation when studying the solitary wavelike solutions in nonlinear dynamics of damped DNA systems.[33]

Likewise, it has been used by Giannini *et al*., Marquie *et al*., and Demiray to analyze the propagation of bright and dark solitons in lossy optical fibers,[34] to study the modulational instability in a real electrical lattice,[35] and to investigate the modulation of nonlinear waves in a thin elastic tube filled with a viscous fluid,[36] respectively.

In the particular case $\sigma = 0$, the discrete version of the eigenvalue problem of Eq. (8), namely,

$$\mathrm{i}\frac{\partial A_n}{\partial \tau} + P(A_{n+1} + A_{n-1} - 2A_n) + Q\,|\,A_n\,|^2\,(A_{n+1} + A_{n-1}) = 0$$

has also been studied by Wen *et al*. in order to further understand the discrete rogue waves phenomena in nonlinear optics and relevant fields.[37] In addition, an extended discrete version of Eq. (8) including the quintic nonlinearity has been used in Ref. [38].

Before ending this subsection, we present in Fig. 4 the behaviors of the dispersion and nonlinear coefficients (P and Q) for values of the wavenumber k chosen in the first Brillouin zone ($0 \le k \le \pi$). These plots show that these coefficients can be positive, null or negative depending on the values of k and the sign of λ. These results are useful for understanding the dynamics and the kind of localized waves that can propagate in the electrical model of MTs considered in this work. Indeed, it is well known that the kind of solutions the NLS equation has strongly depends on the sign of the product of these parameters.[30–32]

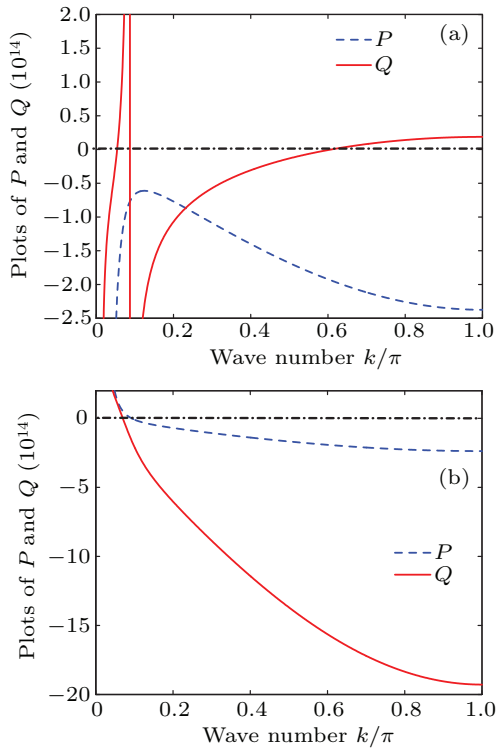


Fig. 4. Nonlinear coefficients and linear dispersive curves as a function of the wavenumber k with the network parameters (4) for the same network parameters as Fig. 2: (a) $\lambda = 4.66 \times 10^{-4}$ ($k_c = 0.043$ rad), (b) $\lambda = -4.66 \times 10^{-4}$.

3.2. Baseband modulational instability

In this section, we focus our attention on the investigation of baseband modulational instability of the amplitude equation (8). To this end, we first consider the plane wave solutions characterized by the time-dependent angular frequency $\Omega(\tau)$, the wavenumber k and the time-varying unperturbed amplitude $A_0 = A_0(\tau)$ in the form[39,40]

$$A(x,\tau) = A_0 \exp[\mathrm{i}(kx - \Omega(\tau))]. \tag{11}$$

Substituting Eq. (11) into Eq. (8), one easily finds that the characteristics of the carrier wave, namely, A_0 and Ω satisfy the following relations:

$$\begin{aligned} \Omega(\tau) &= Pk^2\tau + \frac{Q}{2\sigma}A_0(\tau)^2, \quad \text{if} \quad \sigma \neq 0, \\ \Omega(\tau) &= Pk^2\tau - QA_0(\tau)^2, \quad \text{if} \quad \sigma = 0, \end{aligned} \tag{12}$$

with $A_0(\tau) = A_{00}\exp[-\sigma\tau]$ and $A_0(\tau) = A_{00}$ for $\sigma \neq 0$ and $\sigma = 0$, respectively.

Now, consider a small real phase perturbation of the amplitude ($a(x,\tau)$) and phase ($b(x,\tau)$) as follows:

$$A(x,\tau) = A_0(\tau)[1 + a(x,\tau)]\exp[\mathrm{i}(kx - \Omega(\tau) + b(x,\tau))]. \tag{13}$$

Substituting Eq. (13) into the extended NLS Eq. (8), the linearizing terms give the system

$$\begin{aligned} &\frac{\partial a}{\partial \tau} + 2Pk\frac{\partial a}{\partial x} + P\frac{\partial^2 b}{\partial x^2} = 0, \\ &\frac{\partial b}{\partial \tau} + 2Pk\frac{\partial b}{\partial x} - P\frac{\partial^2 a}{\partial x^2} - 2a{A_0}^2 Q = 0. \end{aligned} \tag{14}$$

We assume that the solutions of Eq. (14) can be written in the form

$$\begin{aligned} a(x,\tau) &= a_0\exp[\mathrm{i}(K_s x - \nu_s\tau)], \\ b(x,\tau) &= b_0\exp[\mathrm{i}(K_s x - \nu_s\tau)], \end{aligned} \tag{15}$$

where K_s and ν_s represent, respectively, the wavenumber and the angular frequency of the perturbation; and a_0 and b_0 are complex constant amplitudes. Substitution of Eq. (15) into Eq. (14) leads to a system of two linear algebraic homogeneous equations for a_0 and b_0. After some algebraic manipulations, the dispersion relation gives

$$(\nu_s - 2qKP)^2 = P^2K_s^2\left(K_s^2 - \frac{2Q}{P}A_0^2\right). \tag{16}$$

The plane wave will be unstable against small modulation if the perturbation diverges with time, that is, the right hand side of Eq. (16) is negative. In this condition, the angular frequency ν_s of the perturbation is complex and its imaginary part is considered as a measure of the growth rate of the perturbation defined as

$$G_m = \left[P^2K_s^2\left(\frac{2Q}{P}A_0^2 - K_s^2\right)\right]^{1/2}, \tag{17}$$

with $PQ>0$ and $K_{\rm s}^2<K_{\rm cr}^2=\frac{2Q}{P}A_0^2$.

Equation (17) shows that the baseband modulational instability of the plane wave (11) occurs if and only if $PQ>0$ and $K_{\rm s}^2<K_{\rm cr}^2$. We note that $K_{\rm cr}$ is an implicit function of the hybrid parameter σ through $A_0(\tau)$. Hence, this parameter can be used to modify the modulational instability region. For instance, for $\sigma>0$, the modulational instability region decreases when the time (τ) increases. On the other hand, for $\sigma<0$, the modulational instability region increases with time τ. Note that, in the particular case $\sigma=0$, the same condition of the modulational instability is obtained but with a constant amplitude ($A_0(\tau)=A_{00}$). These analyses suggest that the ENLS Eq. (8) can admit various solutions including bright solitons ($PQ>0$) and dark solitons ($PQ<0$) to name a few. These solutions will be constructed in the next section.

4. Exact and approximate modulated solitary waves in the network of Fig. 2

In the present section, we focus our attention on the derivation of the exact and approximate representations of the solitary wave solutions of Eq. (8) which correspond to localized wave solutions of Eq. (3). We first note that in the particular case $\sigma=0$, Eq. (8) becomes a standard integrable NLS equation and admits both bright and dark as solitary wave solutions. However, for $\sigma\neq0$, Eq. (8) becomes no longer integrable. Thus, to proceed with the integration of this equation, we introduce the following ansatz:

$$\begin{aligned}&A(x,\tau)=\chi(\tau)U(z)\exp[\mathrm{i}(Kx-\phi(\tau))],\\&z=\varphi(\tau)(x-\nu\tau),\end{aligned}\tag{18}$$

where ν and K are real constants; $\phi(\tau)$ and $\varphi(\tau)$ are the real functions of variable τ to be determined; $U(z)$ is a real envelope function. Substituting Eq. (18) into Eq. (8), we expand and factor out the exponential factor. Then, using a prime to denote a differentiation with respect to z, we obtain the following equations from the imaginary and real parts, respectively:

$$\left(\frac{\mathrm{d}\chi}{\mathrm{d}\tau}+\chi\sigma\right)U-(\nu-2PK)\chi U'+\frac{\mathrm{d}\varphi}{\mathrm{d}\tau}zU'=0,\tag{19}$$

$$P\varphi^2U''+Q\chi^2U^3+\left(\frac{\mathrm{d}\phi}{\mathrm{d}\tau}-PK^2\right)U=0.\tag{20}$$

Now, let $\mathrm{d}\varphi/\mathrm{d}\tau=0$, and Eq. (19) is satisfied for any $U(z)$ by asking that the coefficients of U and U' in this equation vanish, i.e., $\frac{\mathrm{d}\chi}{\mathrm{d}\tau}+\chi\sigma=0$ and $\nu-2PK=0$. This gives rise to the following expressions for χ and ν:

$$\chi(\tau)=\chi_0\exp[-\sigma\tau],\quad \nu=2PK,\quad \varphi(\tau)=\varphi_0,\tag{21}$$

where χ_0 and φ_0 are the real constants, and ν is envelope velocity. Considering Eq. (18), the solution of Eq. (8) can be rewritten as

$$\begin{aligned}&A(x,\tau)=\chi_0\exp[-\sigma\tau]U(z)\exp[\mathrm{i}(Kx-\phi(\tau))],\\&z=\varphi_0(x-2PK\tau),\end{aligned}\tag{22}$$

in which $U(z)$ verifies

$$P\varphi^2U''+Q\chi^2U^3+\left(\frac{\mathrm{d}\phi}{\mathrm{d}\tau}-PK^2\right)U=0.\tag{23}$$

Hence, the initial partial differential equation in the complex variable $A(x,\tau)$ is now reduced to a single second order ordinary differential equation in the real amplitude $U(z)$ given by Eq. (23). In the literature, many powerful techniques have been used to solve such an equation, and several types of solutions have been constructed.[41–50] Here, with the aid of the direct method, our attention is focused on the derivation of the solitary wave solutions of this equation. The kind of these solutions strongly depends on the sign of the product PQ as discussed below.

4.1. Bright-like solitary wave

Here, we are concerned with the investigation of the bright-like soliton solution of Eq. (8). This type of solution exists when $PQ>0$. For this purpose, we introduce the soliton solution of Eq. (23) in the form $U(z)=1/\cosh(\rho z)$. Substituting this ansatz into Eq. (23) and setting the coefficients of the obtained polynomial (in the cosh term) equal to zero, we get the following results:

$$\begin{aligned}&\rho=\frac{\chi}{\varphi_0}\sqrt{\frac{Q}{2P}},\\&\phi(\tau)=\left(PK^2-\frac{Q\chi_0^2}{2}\right)\tau,\quad \text{if}\quad \sigma=0,\\&\phi(\tau)=PK^2\tau+\frac{Q\chi_0^2}{4\sigma}\mathrm{e}^{-2\sigma\tau}+\phi_0,\quad \text{if}\quad \sigma\neq0.\end{aligned}\tag{24}$$

By means of these results, the solution of Eq. (20) can be written as $U(z)=\cosh\left(\frac{\chi}{\varphi_0}\sqrt{\frac{Q}{2P}}z\right)^{-1}$. Using this expression with the regularity condition $\varphi(\tau=0)=0$, i.e., $\varphi_0=-(Q\chi_0^2)/(4\sigma)$, the soliton solution (22)) can be rewritten as

$$A(x,\tau)=\frac{\chi_0\exp\left[\mathrm{i}\left(Kx-\left(PK^2-\frac{Q\chi_0^2}{2}\right)\tau\right)\right]}{\cosh\left(\chi_0\sqrt{\frac{Q}{2P}}(x-2PK\tau)\right)},\quad \text{if}\quad \sigma=0,\tag{25a}$$

$$A(x,\tau)=\frac{\chi_0\mathrm{e}^{-\sigma\tau}\exp\left[\mathrm{i}\left(Kx-PK^2\tau-\frac{Q\chi_0^2}{4\sigma}\left(\mathrm{e}^{-2\sigma\tau}-1\right)\right)\right]}{\cosh\left(\chi_0\mathrm{e}^{-\sigma\tau}\sqrt{\frac{Q}{2P}}(x-2PK\tau)\right)},\quad \text{if}\quad \sigma\neq0.\tag{25b}$$

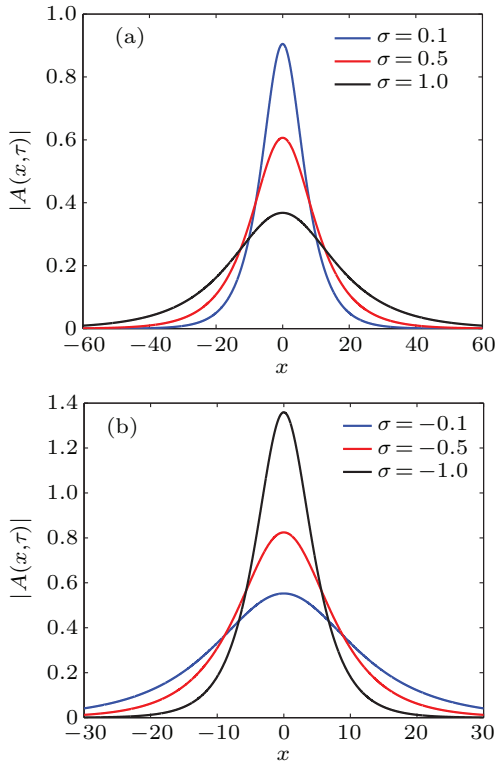


Fig. 5. Effects of the dissipative parameter on the shape of bright soliton (25) at $\tau = 1$, $k = 0.5\pi$ and for the same network parameters as in Fig. 3(a).

Equation (25) shows clearly that for $\sigma = 0$, the analytical expression of the bright-like soliton width is inversely proportional to the soliton amplitude χ_0 which is an independent function of time. It is the most crucial property of the bright soliton. On the other hand, when $\sigma \neq 0$, the soliton amplitude is proportional to function $\exp[-\sigma\tau]$, while its width is inversely proportional to function $\exp[-\sigma\tau]$. This result means that both the amplitude and width of a solitary wave can be manipulated by controlling the parameter σ through resistance elements of the network, as can be seen in Fig. 5. Specifically, for $\sigma > 0$, function $\exp[-\sigma\tau]$ decreases when σ increases, the soliton width increases, and the soliton amplitude decreases (see Fig. 5(a)). In this case, σ is a dissipation parameter. When $\sigma < 0$, function $\exp[-\sigma\tau]$ increases when σ decreases, the soliton width decreases and the soliton amplitude increases (see Fig. 5(b)). Hence, in contrast with the preceding case, σ is an amplification parameter. These observations show that the parameter σ is a hybrid parameter and can be used to control the shape of the bright solitary wave solution.

4.2. Dark solitary wave

When $PQ < 0$, the equation (20) admits a modulated dark solitary wave as a solution. To derive the exact expression of this solution, we consider the following ansatz $U(z) = \tanh(\rho z)$. Substitution of this solution into Eq. (23) and setting the coefficients of the obtained polynomial equal to zero leads to a system of algebraic equations for ρ and $\phi(\tau)$. Solving this system of algebraic equations yields the following results:

$$\begin{aligned}
&\rho = \frac{\chi}{\varphi_0}\sqrt{-\frac{Q}{2P}},\\
&\phi(\tau) = \left(PK^2 - Q\chi_0^2\right)\tau, \quad \text{if} \quad \sigma = 0,\\
&\phi(\tau) = PK^2\tau + \frac{Q\chi_0^2}{2\sigma}\,\mathrm{e}^{-2\sigma\tau} + \phi_0, \quad \text{if} \quad \sigma \neq 0. \qquad (26)
\end{aligned}$$

Based on the above equation, we have $U(z) = \tanh\left(\frac{1}{\delta_0}\sqrt{-Q/(2P)}z\right)$. Using the condition $\varphi(\tau) = 0$, i.e., $\varphi_0 = -(Q\chi_0^2)/(2\sigma)$, the expression of $A(x,\tau)$ can be easily written as

$$A(x,\tau) = \chi_0 \tanh\left(\chi_0\sqrt{-\frac{Q}{2P}}(x - 2PK\tau)\right)\exp\left[\mathrm{i}\left(Kx - \left(PK^2 - Q\chi_0^2\right)\tau\right)\right], \quad \text{if} \quad \sigma = 0, \qquad (27a)$$

$$A(x,\tau) = \chi_0\,\mathrm{e}^{-\sigma\tau}\tanh\left(\chi_0\,\mathrm{e}^{-\sigma\tau}\sqrt{-\frac{Q}{2P}}(x - 2PK\tau)\right)\exp\left[\mathrm{i}\left(Kx - PK^2\tau - \frac{Q\chi_0^2}{2\sigma}\left(\mathrm{e}^{-2\sigma\tau} - 1\right)\right)\right], \quad \text{if} \quad \sigma \neq 0. \qquad (27b)$$

Equation (27) represents the dark soliton solution of the amplitude equation (8) governing the dynamics of modulation in our studied system. It should be noted that, as in the previous case, the characteristic parameters (amplitude and width) of this solution are also the function of $\exp[-\sigma\tau]$. Consequently, it has similar behavior when the sign or value of the parameter σ changes. Thus, the width and the amplitude of the dark solitary wave can be controlled by reducing or increasing the value of the parameter σ. This effect is more clearly seen in Fig. 6, where the shape of the dark soliton (27) is portrayed for different values of σ.

Before ending this subsection, it is important to make some remarks concerning the above obtained solutions. In fact, in the particular case of $\sigma \neq 0$, the obtained solutions Eqs. (27b) and (25b) are the approximate solutions of Eq. (8). They show how the amplitude of solitary waves increases/decreases in time parameter τ as they progress. In the particular case where the hybrid coefficient σ is vanishingly small, one can approximate $\chi(\tau) = \chi_0$ and $\mathrm{e}^{-2\sigma\tau} = 1 - 2\sigma\tau$. Thus, these approximate solutions (27b) and (25b) degenerate to exact solutions (27a) and (25a), respectively.

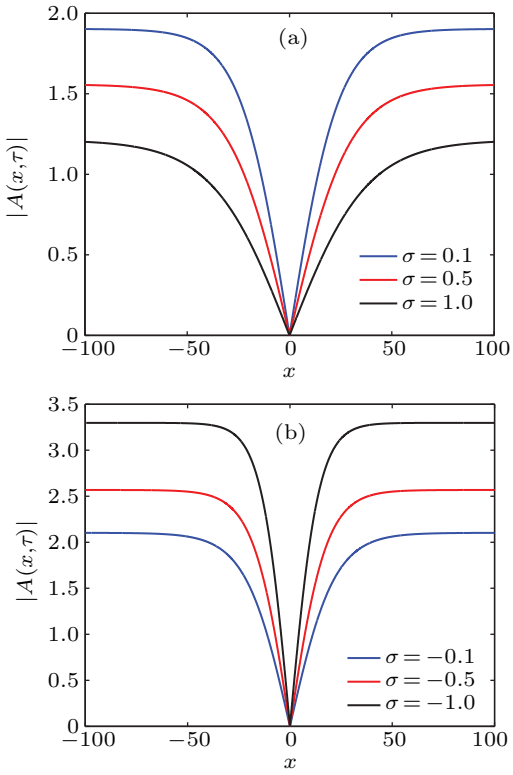


Fig. 6. Effects of the dissipative parameter on the shape of dark soliton (27) at $\tau = 0.5$, $k = 0.61\pi$ and for the same network parameters as in Fig. 3(a).

5. Behavior of modulated waves through the network of Fig. 2.

In the previous sections, the bright and dark solitary wave solutions of the extended nonlinear Schrödinger equation governing the dynamics of the electrical model of microtubules have been obtained. In order to check these analytical calculations, we analyze in the current section the behavior of these waves through the network of Fig. 2 for the wave numbers chosen in the first Brillouin zone. More precisely, we investigate the effects of the parameter σ on the shape of the solitary and rogue wave signals through the system, respectively. To this end, we first express the obtained solutions of the ENLS equation in terms of the network coordinates n and t. In fact, considering dc and second-harmonic terms given by Eq. (7), the voltage signal solution (6) can easily be written as

$$V_n(t) = 2\varepsilon \mathrm{Re}\left[A(x,\tau)\,\mathrm{e}^{\mathrm{i}\theta} + \varepsilon Q_1 A(x,\tau)^2\,\mathrm{e}^{\mathrm{i}2\theta}\right], \tag{28}$$

in which $\theta = kn - \omega t$, $x = \varepsilon(n - \mu t)$ and $\tau = \varepsilon^2 t$. ω and μ are defined by Eq. (5) and represent the angular frequency and group velocity, respectively. $A(x,\tau)$ corresponds to one of the above profiles, namely, the bright solitary solution (25) or the dark solitary solution (27). Next, for the effectiveness of these simulations, the network parameters (4) are exploited together with $\varepsilon = 0.1$ and $\chi_0 = 1$. For given wave number k, we evaluate the frequency ($f = \omega/(2\pi)$) and the group velocity of the wave using Eq. (5), the dispersion and nonlinear coefficients using Eq. (9), and the threshold linear resistance R_{cr} using Eq. (10). The number of cells in the system is taken as equal to $N = 2500$. Thus, we present in Figs. 7 and 8 the evolution of the obtained solitary wave voltage signals.

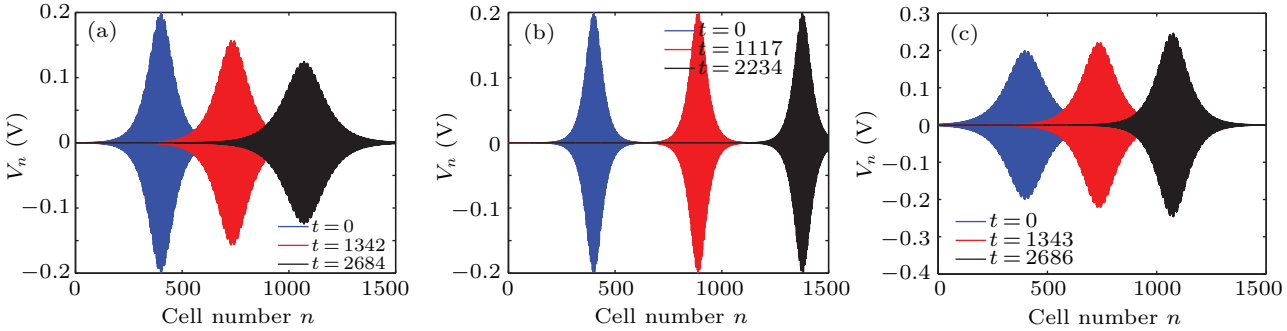


Fig. 7. Signal voltage obtained with the exact bright soliton solution (25) of the dissipative NLS Eq. (8) at different times (in units of ω^{-1}) with network parameters (4) and for $k = 0.5\pi$: (a) $R = 3R_{\mathrm{cr}}$ ($\sigma > 0$); (b) $R = R_{\mathrm{cr}}$ ($\sigma = 0$); (c) $R = 0.1R_{\mathrm{cr}}$ ($\sigma < 0$).

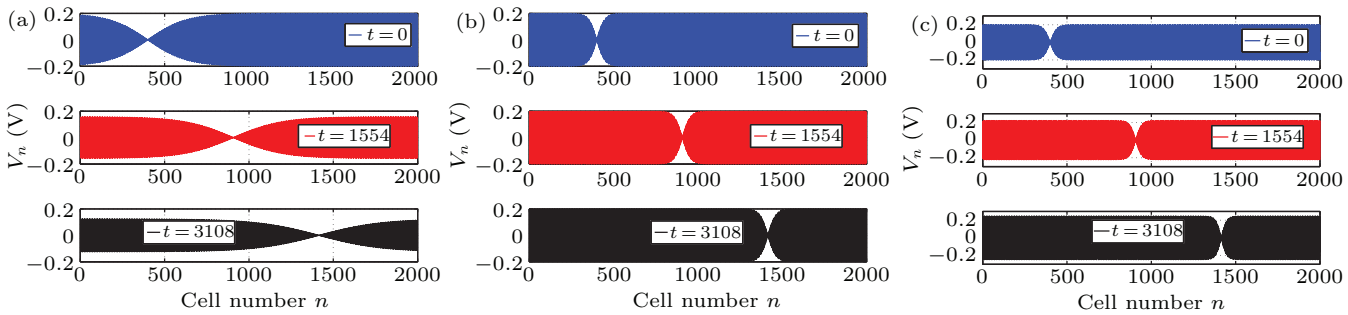


Fig. 8. Signal voltage obtained with the exact dark soliton solution (27) of the dissipative NLS Eq. (8) at different times (in units of ω^{-1}) with network parameters (4) and for $k = 0.61\pi$: (a) $R = 3R_{\mathrm{cr}}$ ($\sigma > 0$); (b) $R = R_{\mathrm{cr}}$ ($\sigma = 0$); (c) $R = 0.1R_{\mathrm{cr}}$ ($\sigma < 0$).

Figure 7 displays the shapes of the bright solitary wave voltages at different times given in units of ω^{-1}. It appears from these figures that the wave amplitude decreases while its width increases when the hybrid parameter σ is positive (Fig. 7(a)). For $\sigma = 0$, that is, the effect of linear resistance is counterbalanced by the effect of the nonlinear resistance, the bright signal voltage propagates in the system with constant amplitude, with constant width, and without distortion of shape (Fig. 7(b)). For $\sigma < 0$, one can see that the amplitude of the wave increases progressively during propagation (Fig. 7(c)). The results are in full agreement with the theoretical prediction, and also corroborate the experimental results obtained in Refs. [7,24]. In addition, as we see in Fig. 8, similar results are obtained with dark solitary waves.

6. Conclusion

In this paper, we have studied the dynamics of modulated waves in an electrical model of a microtubule with linear and nonlinear dissipative elements. Based on the linear dispersion relation, we have shown that the system can behave like a low bandpass filter or a bandpass filter depending on the sign of the conductance's contribution parameter λ to the angular frequency. We have also shown that the allowed bandwidth frequencies of the network strongly depend on the parameter λ.

Applying the reductive perturbation method, we have shown that the well-known nonlinear Schrödinger equation extended by a linear term proportional to a hybrid parameter governs the motion of modulated waves in the network. The sign of this hybrid coefficient σ strongly influences the dissipation/amplification nature of the ENLS equation. We have also shown that the sign of the linear group velocity dispersion and the self-phase modulation coefficients depends on λ.

Likewise, we have derived the exact and approximate solitary wave solutions of the obtained ENLS equation and their dynamics through the network that has been investigated. Our result has revealed that the amplitude and the width of the obtained solitary waves can be controlled based on the parameter σ. In other words, σ can be used to dissipate, stabilize, or amplify the solitary signals propagating through the network.

Finally, the interesting results obtained in this work clearly reveal the significant role of the nonlinear resistance in the electrical model of MTs. In fact, this element can be used to obtain different behaviors (dissipation or amplification) and different characteristics (low bandpass filter or bandpass filter) of the system. In the existing works, each one of these characters or behaviors has been examined in a specific model. Since the electrical model of MTs investigated in the present work adopts alternately the above cited characters or behaviors, we named it the "hybrid" electrical model of MTs. Another interesting aspect of this work is the fact that it can be useful in making a better choice of network parameters and in better understanding the results of experiments of the propagating electrical signal in MTs.

References

[1] Hie B L, Yang K K and Kim P S 2022 *Cell Systems* **13** 274
[2] Sirbu B, Couch F and Cortez D 2012 *Nat. Protoc.* **7** 594
[3] Priel A, Tuszynski J A and Woolf N J 2010 *J. Biol. Phys.* **36** 3
[4] Tuszynski J A, Brown J A, *et al*. 2005 *Math. Comput. Model.* **41** 1055
[5] Havelka D, Cifra M, *et al*. 2011 *J. Theor. Biol.* **286** 31
[6] Kucera O and Havelka D 2012 *BioSystems* **109** 346
[7] Priel A, Ramos A J, Tuszynski J A and Cantiello H F 2006 *Biophys. J.* **90** 4639
[8] Minoura I and Muto E 2006 *Biophys. J.* **90** 3739
[9] Freedman H, Rezania V, Priel A, *et al*. 2010 *Phys. Rev. E* **81** 051912
[10] Havelka D, Cifra M and Kucera O 2014 *Appl. Phys. Lett.* **104** 243702
[11] Zdravkovic S, Bugay A N, Aru G F and Maluckov A 2014 *Chaos* **24** 023139
[12] Zdravkovic S, Sataric M V, Maluckov A and Balaz B 2014 *Appl. Math. Comput.* **237** 227
[13] Tuszynski J A, Portet S, Luxford J M and Cantiello H F 2004 *Biophys. J.* **86** 1890
[14] Priel A and Tuszynski J A 2008 *Europhys. Lett.* **83** 68004
[15] Ilic D I, Sataric M V and Ralevic N 2009 *Chin. Phys. Lett.* **26** 073101
[16] Sataric M V, Ilic D I, *et al*. 2009 *Eur. Biophys. J.* **38** 637
[17] Sataric M V, Sekulic D and Zivanov M 2010 *J. Comput. Theor. Nanosci.* **7** 2281
[18] Sekulic D L, Sataric B M, Tuszynski J A and Sataric M V 2011 *Eur. Phys. J. E* **34** 49
[19] Sataric M V, Sekulica D L, Sataric B M and Zdravkovic S 1015 *Prog. Biophys. Mol. Biol.* **119** 162
[20] Ndjomatchoua F T, Tchawoua C, *et al*. 2016 *Chaos* **26** 053111
[21] Ghomsi P G, Berinyoh J T T and Kakmeni F M M 2018 *Chaos* **28** 023106
[22] Ndzana F II and Mohamadou A 2019 *Chaos* **29** 013116
[23] Mvogo A, Ndzana F II and Kofane T C 2019 *Wave Motion* **84** 46
[24] Priel A, Ramos A J, Tuszynski J A and Cantiello H F 2008 *J. Biol Phys.* **34** 475
[25] Deffo G R, Yamgoué S B and Pelap F B 2021 *Chaos Soliton Fract.* **152** 111397
[26] Deffo G R, Yamgoué S B and Pelap F B 2018 *Phys. Rev. E* **98** 062201
[27] Essimbi B Z and Jäger D 2005 *Current Applied Physics* **5** 567
[28] Jaeger D, Kalinowski D, *et al*. 2007 *Microw. Opt. Technol. Lett.* **49** 2907
[29] Fonkoua S A T, Ngounou S M, Deffo G R, *et al*. 2020 *Chin. Phys. B* **29** 030501
[30] Pelab F B, Kofané T C, Flytzanis N and Remoissenet M 2001 *J. Phys. Soc. Jpn* **70** 2568
[31] Kengne E, Lakhssassi A and Liu M M 2015 *Phys. Rev. E* **91** 062915
[32] Kengne E 2021 *Eur. Phys. J. Plus* **136** 266
[33] Okaly J B, Ndzana II F, Woulaché R L and Kofané TC 2019 *Eur. Phys. J. Plus* **134** 598
[34] Giannini J A and Joseph R I 1990 *IEEE J. Quantum Electron* **26** 2109
[35] Marquié R, Bilbault J M and Remoissenet M 1995 *Physica D* **87** 371
[36] Demiray H 2003 *Appl. Math. Comput.* **145** 179
[37] Wen X Y and Yan Z 2018 *J. Math. Phys.* **59** 073511
[38] Wen X Y, Yan Z and Malomed B A 2016 *Chaos* **26** 123110
[39] Kengne E and Lakhssassi A 2022 *Chaos Soliton Fract.* **160** 112239
[40] Wen X Y and Yan Z 2015 *Chaos* **25** 123115
[41] Cui W N, Zhu Y Y and Li H X 2010 *Chin. Phys. Lett.* **27** 114101
[42] Xu Q and Qiang T 2009 *Chin. Phys. Lett.* **26** 070501
[43] Xu Q and Qiang T 2010 *Chin. Phys. Lett.* **27** 020505
[44] Xu Q and Qiang T 2009 *Chin. Phys. Lett.* **26** 040501
[45] Huang L F, Li Y L, Ni M Y, *et al*. 2009 *Acta Phys. Sin.* **58** 306 (in Chinese)
[46] Xie Z D, Xia C, *et al*. 2019 *Chin. Phys. B* **28** 077501
[47] Xiang Z, Tang C and Yan L 2019 *Chin. Phys. B* **28** 048701
[48] Yamgoué, Deffo G R, Tala-Tebue E and Pelap F B 2018 *Chin. Phys. B* **27** 126303
[49] Yamgoué, Deffo G R, Tala-Tebue E and Pelap F B 2018 *Chin. Phys. B* **27** 096301
[50] Su W, Xie J, Wu T, *et al*. 2018 *Chin. Phys. B* **27** 097501